Wind-tunnel experiments on a large-scale Flettner rotor

Bordogna, G.; Muggiasca, S.; Giappino, S.; Belloli, M.; Keuning, J. A.; Huijsmans, R. H.M.; van't Veer, A. P.

Important note
To cite this publication, please use the final published version (if applicable).
Please check the document version above.

Wind-Tunnel Experiments on a Large-Scale Flettner Rotor

G. Bordogna[1]($\boxtimes$), S. Muggiasca[2], S. Giappino[2], M. Belloli[2],
J. A. Keuning[1], R. H. M. Huijsmans[1], and A. P. van't Veer[1]

[1] Section of Ship Hydromechanics, Delft University of Technology,
Mekelweg 2, 2628 CD Delft, The Netherlands
{g.bordogna, riaan.vantveer}@tudelft.nl
[2] Department of Mechanical Engineering, Politecnico di Milano,
Via la Masa 1, 20156 Milan, Italy
{sara.muggiasca, stefano.giappino,
marco.belloli}@polimi.it

Abstract. Experiments on a large-scale Flettner rotor were carried out in the boundary-layer test section of Politecnico di Milano wind tunnel. The rotating cylinder used in the experimental campaign (referred to as Delft Rotor) had a diameter of 1.0 m and span of 3.73 m. The Delft Rotor was equipped with two purpose-built force balances and two different systems to measure the pressure on the rotor's outer skin. The goal of the experiments was to study the influence of different Reynolds numbers on the aerodynamic forces generated by the spinning cylinder. The highest Reynolds number achieved during the experiments was Re $= 1.0 \cdot 10^6$.

Keywords: Flettner rotor · Rotating cylinder · Magnus effect · Wind power · Wind assisted ship propulsion · Green shipping

1 Introduction

The Flettner rotor is a rotating cylinder that generates an aerodynamic force due to the Magnus effect. Invented by German engineer Anton Flettner, it was first used in 1925 on board the *Backau* ship as a form of propulsion. The *Backau* was equipped with two Flettner rotors and it successfully completed its first voyage across the Atlantic in 1926. The same year, following the success of the first rotor ship, the *Barbara* was launched. The vessel had three Flettner rotors and it served as a freighter in the Mediterranean between 1926 and 1929. Despite the proven concept, the rotor ship was fast abandoned since it could not compete with the increasing adoption of diesel engines and with the very low oil price of that time. In more recent years, however, the possibility to use wind energy as an auxiliary form of propulsion for commercial ships has again become of interest due also to the ever-stringent environmental regulations. Since its inception the Flettner rotor was seldom used for real-life applications in the maritime field, nonetheless the physical phenomena associated to rotating cylinders attracted the interest of many scientists over the past years.

Professor Lafay reported the earliest investigation on the Magnus effect in 1912 (Lafay 1912). The experiments comprised a set of two-dimensional tests during which the aerodynamic forces generated by a rotating cylinder were measured. The author also measured the pressure distribution on the cylinder by employing an external stationary probe placed near the cylinder's surface. Twelve years after, at the NASA Langley Memorial Aeronautical Laboratory, Reid (1924) carried out a systematic series of experiments on spinning cylinders at Reynolds numbers varying between $Re = 3.9 \cdot 10^4$ and $Re = 1.1 \cdot 10^5$. The results of Reid indicated that for the range considered, the Reynolds number had a marginal influence on the aerodynamic forces. The work of Thom represents a major contribution to the research on Flettner rotors. After the completion of his doctoral thesis (Thom 1926), the author worked on a series of reports (Thom 1931; Thom and Sengupta 1932; Thom 1934), that included a vast set of force and pressure measurements of rotating cylinders. The influence of surface roughness, aspect ratio and endplates was investigated. The Reynolds number effect was also studied, although no results for Reynolds numbers greater than $Re = 9.0 \cdot 10^4$ were published. Important to mention is also the pressure measurement system used by the author: an internal manometer tube connected to a spring valve, activated by a cam fixed to the spinning surface and by an external fixed pin. As the cylinder spun, the cam was lifted by the external pin that, by compressing the spring valve, was allowing the manometer tube to measure the pressure at a known position around the cylinder.

Several years after, Swanson (1961) provided a detailed summary of the experiments on rotating cylinders carried out until that time. Results of tests performed by the author for very low velocity ratios (ratio between the incoming flow velocity and the tangential velocity, defined as k), $0 < k < 1$, in the Reynolds number range $3.5 \cdot 10^4 < Re < 5.0 \cdot 10^5$ were also reported. As underlined by Swanson, a remarkable output of his work was the discrepancy in aerodynamic performance of rotating cylinders with different features, and of cylinders with similar features but tested at different Reynolds numbers.

During the oil crisis in the 1980's, wind assistance for ship propulsion was considered an appealing manner to cut operational costs and this led to several publications on the topic. Relevant to the aerodynamic performance of Flettner rotors, are the works of Clayton (1985) and Bergeson and Greenwald (1985). The former author carried out experiments for different numbers of endplates as well as for different Reynolds numbers. Tests were performed in the Reynolds number range $1.7 \cdot 10^4 < Re < 4.9 \cdot 10^4$, and the conclusion was that the Reynolds number had a marked influence on the aerodynamic performance of the Flettner rotor, being the drag coefficient the most affected. On the other hand, Bergeson and Greenwald mounted a 7.2 m tall rotor on aboard of a small motor yacht. Using a combination of mooring lines and spring dynamometers, the authors could measure the forces generated by the rotor for a variety of velocity ratios. The results showed the same trend of previous experiments, however, no details on the Reynolds numbers achieved were given.

Although a different topic, the research carried out on projectiles gives a useful insight on pressure measurement techniques applied on spinning cylinders. Particularly relevant are the studies of Miller (1976), Kayser et al. (1986), Rollstin (1990) and McLaughin et al. (1991). Miller used an internal stationary sliding O-ring seal to

measure the pressure at a given position on the cylinder's surface. The tests were carried out on a cylinder of aspect ratio AR = 1.6 in the range $2.5 \cdot 10^5 < Re < 4.5 \cdot 10^5$ and for velocity ratios up to k = 2. On the other hand, Kayser et al., Rollstin and McLaughin et al. used a transducer attached to the internal surface of the spinning cylinder. The pressure signal was then passed to the readout instrumentation via a transmitter placed inside the cylinder (Kayser et al. and Rollstin) or via a slip ring (McLaughlin et al.).

More recent is the effort of Badalamenti and Prince (2008), who performed a thorough investigation on rotating cylinders using different endplate sizes as well as using rotating or stationary endplates. A series of experiments for a cylinder with no endplate was performed for Reynolds numbers ranging between $Re = 1.9 \cdot 10^4$ and $Re = 9.5 \cdot 10^4$. The results showed that the Reynolds number influenced the lift coefficient for velocity ratios k < 1. At higher values of k, the difference became less pronounced. The use of endplates had a positive effect on the efficiency of the rotating cylinder, particularly in the velocity ratio range $2 < k < 4$.

Other than by experiments, rotating cylinders were also largely studied by means of CFD. In this context, the works of Craft et al. (2012), and Everts et al. (2014) appear to be the most relevant to the present research. Craft et al. performed simulations on a Flettner rotor with and without endplates at three different Reynolds numbers: $Re = 1.4 \cdot 10^5$, $Re = 8.0 \cdot 10^5$ and $Re = 1.0 \cdot 10^6$. The results indicated that the effect of the Reynolds number on the lift coefficient was marginal and no results for the drag coefficient were reported. On the other hand, Everts et al. completed a series of 2D CFD simulations on a rotating cylinder at $Re = 5.0 \cdot 10^5$, $Re = 1.0 \cdot 10^6$ and $Re = 5.0 \cdot 10^6$. The aim was to investigate the influence of the Reynolds number as well as the influence of different surface roughness coefficients on the aerodynamic forces. The results reported showed that both the Reynolds number and the surface roughness have a considerable influence on the lift and drag forces generated.

Other studies, both experimental and numerical, carried out on rotating cylinders and not included in this summary can be found in (Zdravkovich 2003).

The literature review presented shows that despite the numerous studies on rotating cylinders there is still disagreement on the influence of the Reynolds number on the aerodynamic forces generated. Moreover, the experimental efforts reviewed were typically undertaken at low Reynolds numbers, or at higher Reynolds numbers but at low velocity ratios or using cylinders with very low aspect ratios. In this context, the aim of the present research is to contribute to the understanding of the scale effects on the lift and drag forces generated by a Flettner rotor tested at high Reynolds numbers. To be noted that the current work focuses on the various experimental techniques employed during the testing campaign; only a small part of the experimental results is presented. A subsequent article will be published in which the complete set of results is provided with the aim to offer a useful benchmark for CFD validation.

2   Experimental Setup

Two series of tests were performed on the Delft Rotor: in December 2017 and in March 2018. The experiments were carried out in the boundary-layer test section of Politecnico di Milano wind tunnel. The test section is 13.84 m wide, 3.84 m high and 35 m long. The maximum reachable wind speed is 15 m/s and the turbulent index in smooth-flow condition is 2%. The Delft Rotor was mounted in the centre of the chamber, in correspondence with two large I-section beams used as a foundation (Fig. 1).

Fig. 1. The Delft Rotor in the boundary-layer chamber of Politecnico di Milano wind tunnel

The Delft Rotor is a rotating cylinder with diameter D = 1.0 m and span H = 3.73 m and it is comprised of three main parts: a static structure, a rotating frame and an outer skin. The static structure consisted of a lower and an upper steel assembly made of four M30 threaded bars screwed into four bases, that were bolted to the wind-tunnel ground and ceiling I-section beams. To improve the stiffness of the static assemblies, four oblique steel bars were connected to the threaded bars and the force balance (Figs. 3 and 5a).

Two aluminium purpose-built force balances were placed at the extremity of the threaded bars, on top of which the bearing housings were bolted (Figs. 2, 3 and 4). To compensate for a possible misalignment, it was chosen to use two self-aligning spherical roller bearings.

The reason to position the balances close to the bearings was to reduce to the minimum the bending moment. By doing so, it was possible to use a three-component force balance: only lift, drag and torque were measured.

Each force balance was carved out of 30 mm thick aluminium slab and it consisted of two concentric circles connected by four strips on which the lift, drag and torque extensometers were placed (Fig. 4). The force balances were purposely built for the Delft Rotor experiments in order to withstand the large aerodynamic forces expected to act on the cylinder ($Lift_{max} = 2500\ N$).
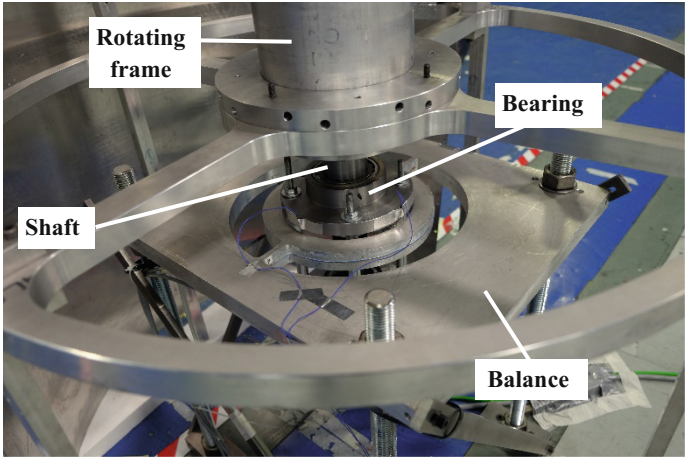
Fig. 2. Lower assembly of the Delft Rotor's static structure
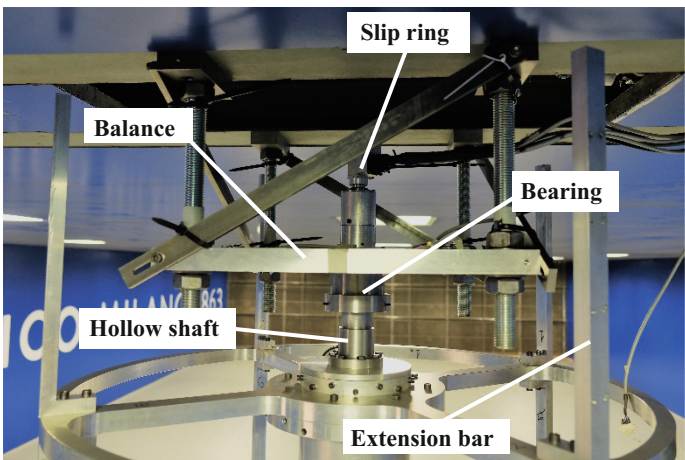
Fig. 3. Upper assembly of the Delft Rotor's static structure

The rotating frame of the Delft Rotor consisted of a 5 mm thick aluminium tube to which three equal aluminium wheels were bolted (Fig. 5a). The wheels were connected with eight vertical bars, and four lower bars (Fig. 5b) and four upper bars (Fig. 3) were used as an extension so that the internal frame matched the height of the outer skin.

The extremities of the internal tube were plugged with lids into which two steel shafts were screwed. The shafts were then fitted into the bearings (Figs. 2 and 3).

The Delft Rotor's outer skin was composed of four calendered aluminium sheets. The sheets were 2 mm thick and they were bolted to the internal frame with more than 250 countersunk head screws. The high number of screws used to secure the calendered sheets to the rotor's internal frame was necessary to achieve a safety factor of 2 while

expecting a maximum centrifugal force of 15 kN (the total weight of the rotating components was 170 kg). The frame was rotated using an electric engine that was hung to the lower bearing housing by means of four threaded bars, and a flexible coupling was used to connect the engine shaft with the lower shaft of the internal frame (Fig. 5b).
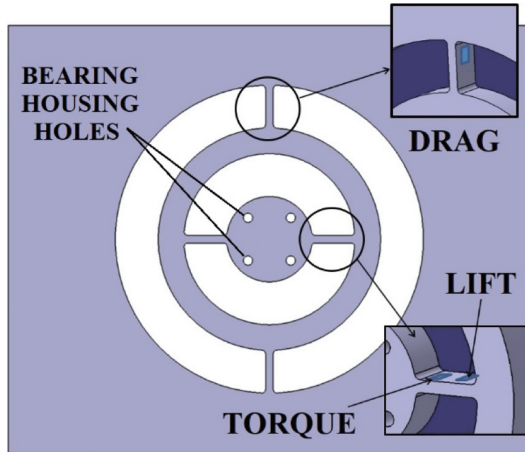
Fig. 4. Three-component force balance used during the experiments
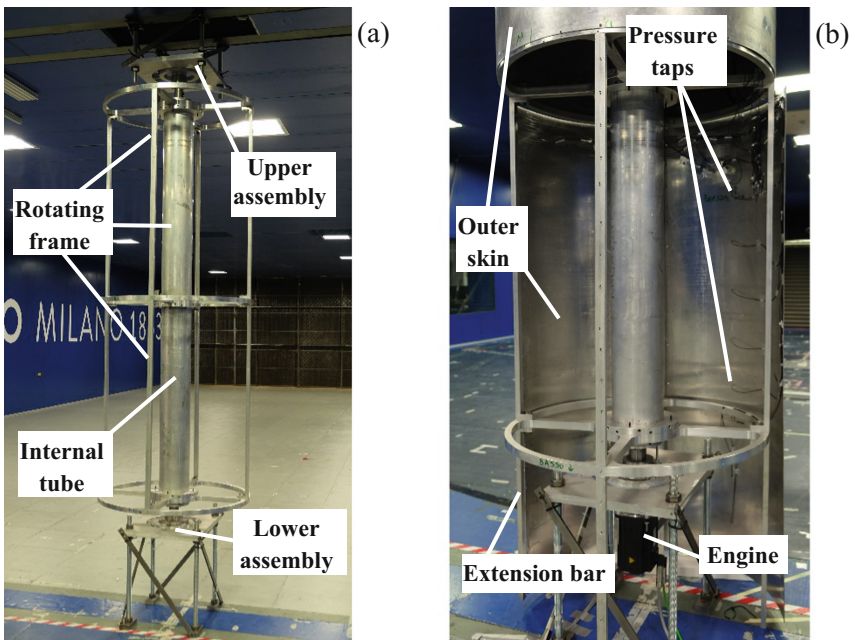
Fig. 5. Internal rotating frame without (a) and with (b) outer skin

The Delft Rotor was equipped with two different pressure measurement systems, namely one high sample-rate pressure scanner (PSI ESP-32HD) with 32 pressure sensors and one single AMS 4711 sensor. The AMS4711 sensor has a pressure range of ±2000 Pa and the ESP scanner of ±2500 Pa. The ESP scanner was mainly installed to be used during the static measurements, whereas during the dynamic experiments was used as redundancy system. During the first series of tests, all 32 pressure taps were equally distributed around the cylinder circumference at 1.85 m from the ground. Doing so, it was possible to measure the pressure distribution around a whole section at the cylinder mid-height.

During the second series of tests, however, 16 taps were removed from the circumference and they were equally spaced along a vertical line (Fig. 5b). This second type of arrangement was used to measure the pressure distribution on the cylinder at different heights. In fact, due to the wind-tunnel boundary layer, the flow speed decreases towards the floor and the ceiling of the chamber. The ESP system comprised a signal conditioner and a pressure scanner. The signal conditioner was fixed to the rotor's internal tube, whereas the pressure scanner was placed on the rotating frame middle wheel as close to the internal tube as possible in order to reduce the centripetal acceleration acting upon it (Fig. 6). The AMS4711 sensor is a very compact pressure instrument (32 × 25 × 13.5 mm) and, due to its minimized dimensions, it was possible to secure it directly to the cylinder inner face.

An advantage of doing so is that the length of the pressure tube was reduced to the minimum. The inner diameter and the length of the pressure tubes in fact have a considerable influence on the frequency response and this is particularly evident at high rotational speeds. Similarly to the ESP system, also the AMS4711 sensor was placed at 1.85 m from the ground (cylinder mid-height). The pressure systems installed on the Delft Rotor use a piezoresistive silicon chip as sensing element and both work as
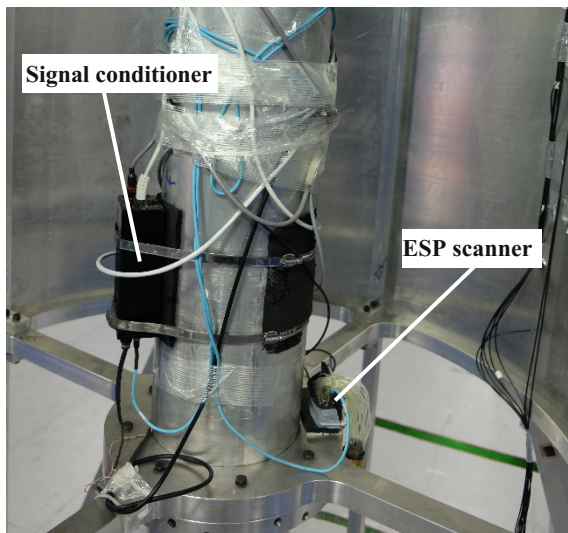
Fig. 6. Position of the ESP scanner and its signal conditioner on the rotating frame

differential transducers. This means that to know the actual pressure acting on the cylinder outer skin, it was necessary to measure also the static pressure in the interior of the cylinder. This was done with a single pressure tube located above the lower force balance. To pass the signal of both the ESP scanner and the AMS4711 sensor to the readout instrumentation, a slip ring connected to the upper hollow shaft was installed (Fig. 3).

The slip ring was also equipped with a transducer to measure the instantaneous velocity and angular position. The angular position of the cylinder was therefore in phase with the pressure measurements.

The experiments were conducted in smooth-flow conditions and the flow velocity was measured with a Pitot tube placed 5 m in front of the Delft Rotor at the height of 1.85 m from the wind-tunnel floor.

3   Pressure Measurement Correction

As mentioned in the previous section, the pressure tube length and inner diameter influence the pressure frequency response as they act as a filter on the signal. This effect is generally relevant in experiments in which the pressures on a moving object need to be measured, and it becomes more noticeable as the speed of the moving object increases. Since the tubes of the 32 pressure taps had to be connected to one single scanner, inevitably they had a considerable length. For this reason, the pressures measured by the ESP scanner had to be corrected to account for the frequency response of the tubing system. During the first series of tests, it was chosen to use tubes of 1.02 mm inner diameter whereas during the second experimental campaign larger tubes with an inner diameter of 1.50 mm were employed. From the analysis of the pressure data, it appeared that the tubes with larger diameter had a better frequency response when compared to the data of the AMS4711 sensor.

Another correction that needs to be applied is to consider the centripetal acceleration acting upon the air column enclosed inside the pressure tubes or acting directly upon the measurement instrument. In the first case, the effect of the acceleration on the air column is dependent on the length of the pressure tubes in the radial direction (not on the total length of the tubes). In the second case, the effect of the acceleration on the measurement instrument is dependent on the distance of the device from the axis of rotation. This means that, due to the way the pressure measurement systems were mounted on the Delft Rotor, the pressures measured by the ESP scanner need to be corrected to account for the effect of the acceleration on the air column enclosed in the pressure tube connecting the scanner and the pressure tap, while the pressures measured by the AMS4711 sensor need to be corrected for the effect of the acceleration acting on the sensor itself. As reported in (Pollack et al. 1972), the effect of the acceleration on the air column can be estimated according to Eq. (1):

$$p_A - p_B = \frac{\rho\omega^2}{2} \cdot \left(r_A^2 - r_B^2\right) \tag{1}$$

where $p_A - p_B$ is the pressure difference between the measurement instrument and the pressure tap, ρ is the air density, ω is the angular velocity and r_A and r_B are the radial

distances of the measurement instrument and the pressure tap from the axis of rotation. To provide an example of the effect of the centripetal acceleration on the pressure measurements, in Fig. 7 the pressures measured with the cylinder spinning at increasing angular velocities in still air are reported.
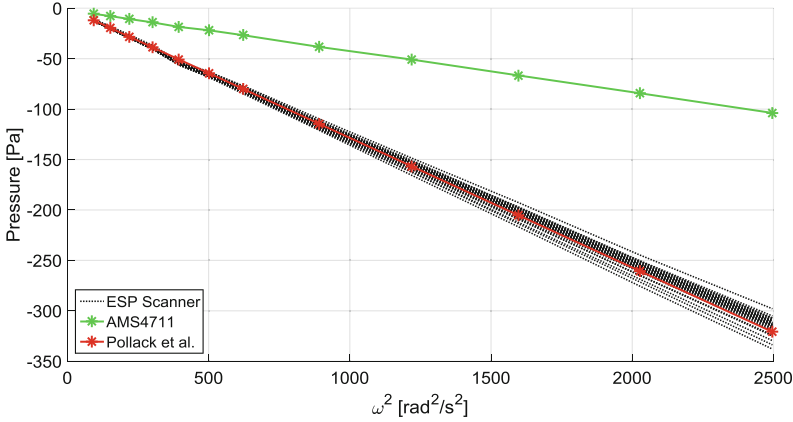
Fig. 7. Measured pressure in still air as a function of the angular velocity squared

The results of Fig. 7 show that the effect of the acceleration is similar for all 32 sensors of the ESP scanner, although the lengths of the pressure tubes are considerably different from one another (390 mm $< L_{tube} < 2500$ mm). The results of the AMS4711 sensor on the other hand, do not follow the same trend as the measured pressure is due to the acceleration acting on the sensing membrane. This effect is described, for instance, in (Kurtz et al. 2003). The authors also provide a simple estimate of the acceleration effect on a generic piezoresistive pressure sensor depending on the magnitude of the acceleration and the full-scale pressure range of the device.

To overcome the issues concerning the correction of the pressure measurements here elaborated, during the experiments the cylinder was spun in still air at the corresponding angular velocity of each subsequent real measurement (rotation + wind switched on). This procedure was repeated for all performed tests. Thus, the pressures measured with both instrumentations were corrected according to:

$$p_{corrected} = [p_{rot.\&wind} - \Delta p_{rot.\&wind}] - [p_{rot.} - \Delta p_{rot.}] \qquad (2)$$

where $p - \Delta p$ is the pressure measured during experiments with wind switched on (*rot.&wind*) or with wind switched off and just the rotation (*rot.*), corrected for the difference in static pressure between inside and outside the cylinder for the corresponding test. By applying this correction, the effects of the acceleration were eliminated irrespective of whether they affected the tubing system or the measurement instrument itself. Nevertheless, using this correction method, also the pressure experienced by the cylinder due to the rotation itself in still air is discarded. The magnitude

of this effect can be estimated by subtracting the averaged pressure measured in still air by the 32 ESP scanner sensors and the results of Eq. (1), (see Fig. 7). Using this procedure, it appears that the pressure due to the rotation itself is negligible as also reported in (Thom 1931).

4   Preliminary Results of the Experiments

The primary aim of the experiments was to investigate the influence of the Reynolds number on the aerodynamic forces generated by the Delft Rotor for different velocity ratios. Nonetheless, static and quasi-static experiments were also performed to check the accuracy of the measurement setup. While during the static tests the cylinder was not rotating, during the quasi-static experiments the cylinder was rotating at very low rpm. This type of experiments aimed at continuously measuring the pressures on the rotor's surface also using the AMS4711 sensor. During the quasi-static tests, the Delft Rotor was span at 2 rpm. This rotational speed was low enough to ensure that the quasi-static assumption with respect to the typical vortex shedding frequency of a cylinder at a given Reynolds number (in this case Strouhal number $St < 0.2$) held true for the entire range of wind speed tested.

As mentioned in the introductory section, the focus of the present work is to prove the validity of the experimental techniques adopted during the tests rather than on the experimental results themselves. For this reason, a comparison between the results obtained with the ESP scanner and with the AMS4711 sensor is provided, using both a static and quasi-static approach. In Figs. 8, 9 and 10 the results for $Re = 2.5 \cdot 10^5$, $Re = 5.2 \cdot 10^5$ and $Re = 9.8 \cdot 10^5$ are reported.
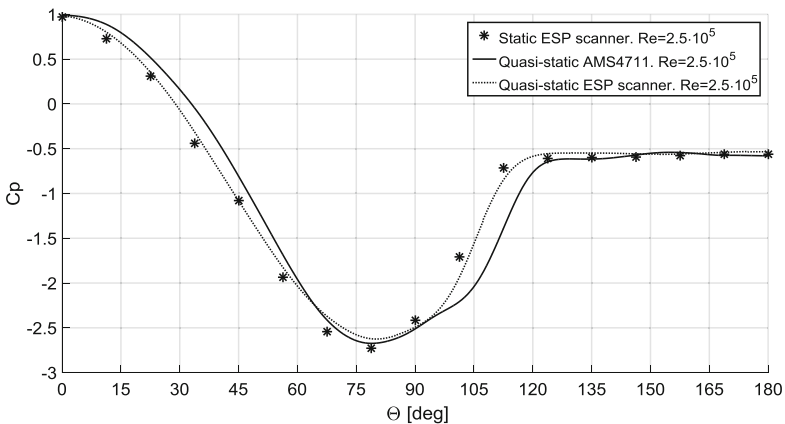
Fig. 8. Mean pressure distribution on the cylinder: static vs quasi-static approach. $Re = 2.5 \cdot 10^5$
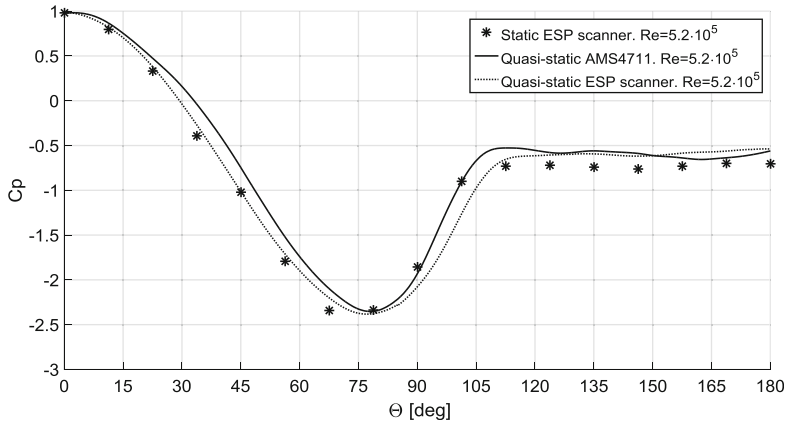
Fig. 9. Mean pressure distribution on the cylinder: static vs quasi-static approach. Re $= 5.2 \cdot 10^5$
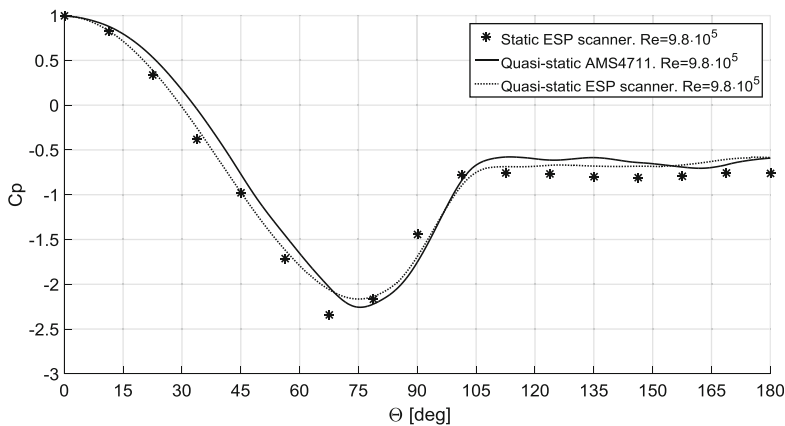
Fig. 10. Mean pressure distribution on the cylinder: static vs quasi-static approach. Re $= 9.8 \cdot 10^5$

The results of the comparison show that the two measurement instruments are in satisfactory agreement, both when a static or quasi-static approach is employed. The pressure distributions over the cylinder for the Reynolds numbers considered are also in line with data reported in (Zdravkovich 2003).

The lift and drag coefficient obtained at Re $= 3.6 \cdot 10^5$ for a set of various velocity ratios are given in Fig. 11. The forces were measured with the force balances as well as by integrating the pressures measured with the 16 sensors of the ESP scanner distributed over the span of the cylinder.

For the lift coefficient, it is shown that there is an excellent agreement between the forces measured by the balances and the results obtained by the pressure integration.
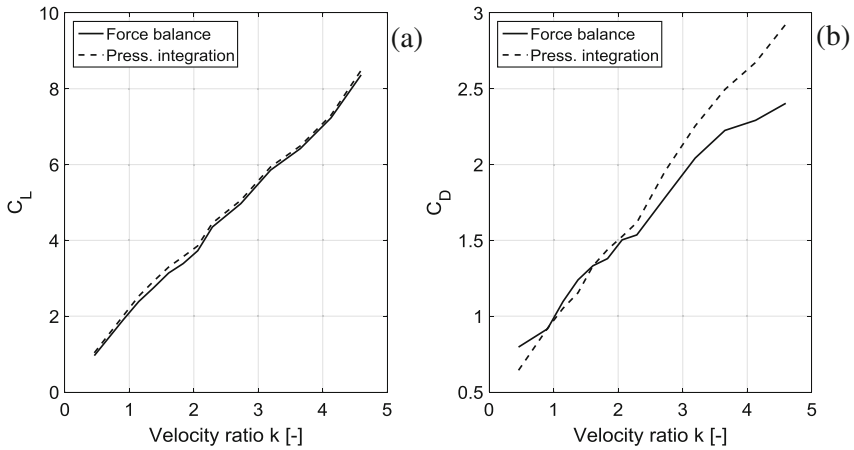
Fig. 11. Lift (a), drag (b) coefficients: measured forces vs pressure integration of ESP scanner data

For the drag coefficient, on the other hand, the agreement is less satisfactory, particularly at high velocity ratios. This is justifiable since the drag component is more sensitive to the orientation of the pressure distribution and, at high rotational speeds, achieving an accurate match between the pressure distribution and the angular position of the cylinder is a challenging task.

Although just a small set of results was published in this section, for the sake of completeness, a summary of all the dynamic experiments carried out on the Delft Rotor is given in Table 1.

Table 1. Summary of the dynamic experiments performed on the Delft Rotor

Date	Re [·10^5]	Velocity ratio k ∨ = executed - = not executed												
		0.5	1.0	1.25	1.5	1.75	2.0	2.25	2.5	3.0	3.5	4.0	4.5	5.0
Dec.'17	1.8	-	∨	∨	∨	∨	∨	∨	∨	-	-	-	-	-
Dec.'17	3.6	-	∨	∨	∨	∨	∨	∨	∨	-	-	-	-	-
Dec.'17	5.5	-	∨	∨	∨	∨	∨	∨	∨	-	-	-	-	-
Dec.'17	10.0	-	∨	∨	∨	∨	∨	-	-	-	-	-	-	-
Mar.'18	1.8	∨	∨	-	∨	-	∨	-	∨	-	-	-	-	-
Mar.'18	2.5	∨	∨	∨	∨	∨	∨	∨	∨	∨	∨	∨	∨	∨
Mar.'18	3.6	∨	∨	∨	∨	∨	∨	∨	∨	∨	∨	∨	∨	∨
Mar.'18	10.0	∨	∨	-	∨	-	∨	-	-	-	-	-	-	-

5 Conclusions

In the present work, a literature review on the experimental efforts conducted on Flettner rotors is provided. From the review, it appears that the effect of the Reynolds number on the aerodynamic forces generated by the rotor is still under discussion and that there is a lack of experimental data obtained at high Reynolds numbers. The experimental campaign on the Delft Rotor carried out at Politecnico di Milano wind tunnel is described in detail, with emphasis on the pressure measurement instruments used. The pressure measurements and the necessary correction to account for the effects of the centripetal acceleration represented one of the major difficulties of the described experiments. Nevertheless, the measurement instruments employed, and the correction methods applied, proved to provide meaningful results.

References

Badalamenti C, Prince SA (2008) The effects of endplates on a rotating cylinder in crossflow. In: 26th AIAA applied aerodynamics conference, Honolulu, HI, USA, 18–21 August

Bergeson L, Greenwald CK (1985) Sail assist developments 1979–1985. J Wind Eng Ind Aerodyn 19:45–114

Clayton BR (1985) BWEA initiative on wind assisted ship propulsion (WASP). J Wind Eng Ind Aerodyn 19:251–276

Craft TJ, Iacovides H, Johnson N, Launder BE (2012) Back to the future: Flettner-Thom rotors for maritime propulsion? In: 7th international symposium on turbulence heat and mass transfer, Palermo, Italy, 24–27 September

Everts M, Ebrahim R, Kruger JP, Miles E, Sharifpur M, Meyer JP (2014) Turbulent flow across a rotating cylinder with surface roughness. In: 10th international conference on heat transfer, fluid mechanics and thermodynamics, Orlando, FL, USA, 14–16 July

Kayser LD, Clay WH, Damico Jr WP (1986) Surface pressure measurements on a 155 mm projectile in free-flight at transonic speed. In: 14th aerodynamic testing conference, West Palm Beach, FL, USA, 5–7 March

Kurtz AD, Ainsworth RW, Thorpe SJ, Ned A (2003) Further work on acceleration insensitive semiconductor pressure sensor for high bandwidth measurements on rotating turbine blades. In: NASA propulsion measurement sensor development workshop, Huntsville, AL, USA, 13–15 May

Lafay A (1912) Contribution Experimentale a l'Aerodynamique du Cylindre. Reveus Mechanique 30:417–442

McLaughlin TE, Stephen EJ, Robinson MC (1991) Pressure measurements on a rotating circular cylinder. AIAA-91-3265-CP

Miller MC (1976) Surface pressure measurements on a spinning wind tunnel model. AIAA J 14:1669–1670

Pollack FG, Liebert CH, Peterson VS (1972) Rotating pressure measuring system for turbine cooling investigations. Technical report TM X-2621, NASA

Reid EG (1924) Tests of rotating cylinders. Technical report TN-209, NACA

Rollstin LR (1990) Measurement of in-flight base pressure on an artillery-fired projectile. J Spacecraft Rockets 27:5–6

Swanson WM (1961) The Magnus effect: a summary of investigations to date. J Basic Eng 83:461–470

Thom A (1926) The aerodynamics of a rotating cylinder. PhD thesis, University of Glasgow, UK

Thom A (1931) Experiments on the flow past a rotating cylinder. Technical report R&M No. 1410, Aeronautical Research Council

Thom A, Sengupta SR (1932) Air torque on a cylinder rotating in an air stream. Technical report R&M No. 1520, Aeronautical Research Council

Thom A (1934) Effects of discs on the air forces on a rotating cylinder. Technical report R&M No. 1623, Aeronautical Research Council

Zdravkovich MM (2003) Flow around circular cylinders, volume 2: applications. Oxford University Press Inc., New York